Proceedings of ASME Turbo Expo 2011
GT2011
June 6-10, 2011, Vancouver, British Columbia, Canada

GT2011-46132

PIV STUDY ON THE DIMPLE MID-PLANE OF A NARROW RECTANGULAR CHANNEL WITH DIMPLES APPLIED TO ONE WALL

Lucky V. Tran, Michelle I. Valentino,
Abhishek Saha, Carson D. Slabaugh,
Mark Ricklick, J.S. Kapat
Center for Advanced Turbines and Energy Research
Laboratory for Turbine Aerodynamics, Heat Transfer, and Durability
University of Central Florida
Orlando, FL USA

Saptarshi Basu
Department of Mechanical Engineering
Indian Institute of Science,
Bangalore, India

ABSTRACT

This paper presents an investigation of the fluid flow in the fully developed portion of a rectangular channel (Aspect Ratio of 2) with dimples applied to one wall at channel Reynolds numbers of 20,000, 30,000, and 40,000. The dimples are applied in a staggered-row, racetrack configuration. Results for three different dimple geometries are presented: a large dimple, small dimple, and double dimple. Heat transfer and aerodynamic results from preceding works are presented in Nusselt number and friction factor augmentation plots as determined experimentally. Using particle image velocimetry, the region near the dimple feature is studied in detail in the location of the entrainment and ejection of vortical packets into and out of the dimple; the downstream wake region behind each dimple is also studied to examine the effects of the local flow phenomenon that result in improved heat transfer in the areas of the channel wall not occupied by a feature. The focus of the paper is to examine the secondary flows in these dimpled channels in order to support the previously presented heat transfer trends. The flow visualization is also intended to improve the understanding of the flow disturbances in a dimpled channel; a better understanding of these effects would lead the development of more effective channel cooling designs.

INTRODUCTION

Advancements in cooling technology for gas turbines are continuously investigated to increase the turbine engine inlet temperature without compromising materials' durability to effectively enhance the gas turbine efficiency. One area of interest where cooling methods are introduced is the turbine blade. Some cooling schemes used within the turbine blade include: film cooling through discrete holes on the surface of the blade, impingement cooling, and transport enhancement techniques to promote heat transfer on the internal cooling channels within the blade. A variety of geometries have been introduced as surface enhancements for internal cooling channels; the added roughness of the surface geometries break up the laminar sub-layer of the channel flow and promote mixing and secondary flows throughout the channel. Transport-enhancing features such as ribs, pin fins, swirl chambers, scales, and dimples have all been reviewed for contribution to mixing and secondary flows.

The application of dimples can be seen as early as 1966, where Snedeker and Donaldson carried out an experimental study on flow inside of a hemispherical cavity [1]. Although this had more aerodynamic applications, the idea of using a dimpled surface to promote heat transfer followed with a further characterization of the flow behavior by Murzin et al. [2]. Belen'kiy et al. used a staggered array of surface indentions to improve heat transfer in a shell and tube heat exchanger [3]. Other designs of the dimples included a tear-drop shape; this design was experimented and complared with the hemispherical concavity using transient TLC by Chyu et al. [4]. Moon et al. studied turbulent heat transfer measurements on a wall with concave and cylindrical dimples in a square channel [5].

Dimpled surfaces are becoming more prevalent in current studies because of their ability to promote mixing of the flow without creating high pressure losses through the channel. A concavity approach for use in compact heat exchangers was studied by Chyu et al. [6]. The effect of channel height on heat transfer and friction in dimpled cooling passages was studied by Moon et al. [7]. Mahmood and Ligrani studied the effect of aspect ratio, temperature ratio, and Reynolds number on the flow structure and heat transfer in a dimpled array [8]. Burgess et al. discussed Nusselt number behavior on deep dimpled surfaces [9]; Burgess and Ligrani studied effects of dimple depth for Nusselt numbers and friction factors for an array of dimples, concluding that the highest heat transfer ratios were found at the downstream dimple edge and the flat surface just downstream of the dimple [10, 11]. Results of numerical

solutions of turbulent convective heat transfer with a single spherical dimple were then presented by Isaev et al. [12]. Applying dimples to rotating machinery, Griffith et al. studied the effects of rotation of a rectangular channel with dimples applied to two walls [13].

Zhao compared the friction coefficient in smooth walled channel to a dimpled channel finding the difference to be within the range of experimental uncertainty [14]. Borisov et al. presented a "banked" dimple and protrusion design and reported heat transfer and pressure loss through the channel [15]. Borisov et al. also studied heat transfer and pressure losses in a narrow dimpled-protrusion channel for application in a recuperator core [16]. Effects of combined dimpled/protrusion walls on thermal performance inside a channel at low Reynolds numbers were then examined by Hwang et al. [17]. Leinhart et al. performed both numerical and experimental analysis of turbulent flow over a dimpled surface to determine the effect on skin-friction drag [18]. Recent studies varying dimensions or overall shape of the dimple to review the effects on heat transfer and friction augmentation include Isaev et al. who studied the dimple depth on these effects [19]. Leontiev et al. also conducted a numerical study of turbulent air flow and heat transfer for a narrow channel [20]; the channel height was varied while maintaining the dimple shape, and then the dimple diameter was varied while maintaining a constant channel cross section. Leontiev et al. also looked at oval, conical, and spherical dimples with varying dimple depth.

Slabaugh et al. studied altering the dimple shape or footprint, looking at two dimple footprint diameters as well as a double-dimpled feature and the effect the dimples produce on the side walls of a small aspect ratio channel (AR=2) using a modular copper block test section implemented with thermocouples [21]. This study concluded the double dimple shape produced a higher heat transfer augmentation at a much lower cost of pressure drop in the channel. Slabaugh et al. then performed transient TLC measurements on an upscaled acrylic channel to obtain local heat transfer coefficients on all four walls of the channel [22]. The double-dimple shape was further reviewed by Slabaugh for his work using numerical modeling through LES [23].

The change in shape from a single dimple to a double dimple creates an increase in the streamwise length. The double dimple incorporates two spherical dimples into one feature, creating a ridge between the upstream and downstream dimple that does not exist in a single dimple feature. The presence of this ridge may disrupt the flow and reduce the size of the recirculation zone. In addition, the increased streamwise length of the feature allows for the flow to enter and exit the dimple more gradually (no large angle ejection) and has a better reattachment than seen in the single dimple (see Fig. 1).

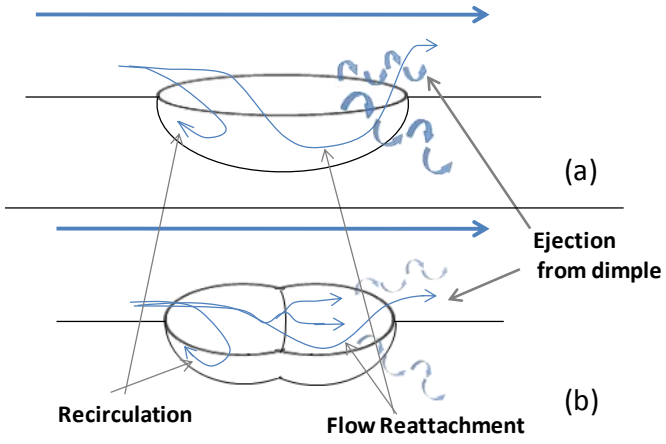

Figure 1: Flow Structures in a (a) Single Dimple (b) Double Dimple

Experimental investigations of the flow field in a dimpled channel are exceedingly rare and none for the double dimple exist. Mahmood et al. [24] used a Kiel and static pressure probe to measure time-averaged velocity components and pressure distributions in the spanwise-normal plane. Won et al. [25] and Ligrani et al. [26] both used smoke visualization at low Reynolds number and a five-hole probe to measure the time averaged velocity and pressure distribution in the spanwise-normal plane, Constant Temperature Anemometry was also used to map the longitudinal velocity fluctuation distribution along the channel height. In those studies, CTA measurements were performed at two locations, just downstream of the downstream edge of the dimple along the centerline of the dimple and offset from the centerline by half the dimple print diameter.

Terekhov et al. [27,28] performed the most extensive experimental investigations using hydrogen gas bubbles generated through electrolysis for flow visualization and Laser Doppler Anemometry to measure the spanwise distribution of longitudinal velocity above the cavity and the along the channel height at three locations, over the center of the cavity and slightly upstream and downstream of the cavity center.

The current study utilizes 2D particle image velocimetry (PIV) to study the flow physics in three different dimple geometries, previously studied by Slabaugh et al. in [21-23], including the first experimental flow visualization performed in a double dimpled channel. The experiments performed will add valuable additional datasets for others studying dimple-induced secondary flows to compare to their works, especially for the purpose of validating LES simulations. The current configuration is significantly different from studies in the past, where either the central dimple of a vast array or the oncoming flow over a single dimple studied. The current experimental setup is able to accommodate no more than one dimple per row (if an analogy to a row or an array is applied) because of the narrow aspect ratio of the channel and dimple parameters used. The periodically fully developed flow in a dimpled, narrow

(relative to the dimple size) channel is the current concern where the dimple-to-dimple and dimple-to-wall interactions are occurring. The interactions between these flow features are not included in typical studies on dimples.

Notwithstanding other quantitative flow measurements near a dimple, the use of PIV for flow visualization has not yet been reported. Even as the present study does not completely settle all questions concerning the complex flow field near a dimple, the presentation and publication of any additional quantitative measurements could contribute additional datasets for others researching dimples to compare to their works. This study utilized PIV in the channel (data within the cavity could not be obtained), being performed for the first time (to the best of the authors' knowledge) in a dimpled channel for internal cooling applications. Furthermore, the concept of the double dimple presented in this paper is entirely new, being conceived originally by the current authors. The measurements being performed are the first quantitative measurements of flow in a channel with double dimples applied.

NOMENCLATURE

Roman Symbols

A	Wetted Area
D, D_h	(Dimple) Diameter, Hydraulic Diameter
d	Dimple Print Diameter
f	Darcy Friction Factor
H	Channel Height
h	Convective Heat Transfer Coefficient
Nu	Nusselt Number
P	SpanwisePitch of dimple array
R	(Dimple) Radius (D/2)
Re	Reynolds Number
S	Streamwise Pitch
t	Time
$\bar{U}$, U'	Mean Velocity
v	Fluid Velocity
W	Channel Width
x	Streamwise coordinate measured from dimple leading edge
y	Normal coordinate measured from dimple horizon
z	Spanwise coordinate

Greek Symbols

δ	Dimple Depth

Abbreviations

AR	Channel Aspect Ratio (W/H)
CCD	Charge Coupled Device
CFD	Computational Fluid Dynamics
CTA	Constant Temperature Anemometry
DD, LD, SD	Double Dimple, Large Dimple, Small Dimple
LES	Large Eddy Simulation
PIV	Particle Image Velocimetry
TLC	Thermochromic Liquid Crystal

Summary of Preceding Work

The current study was preceded by heat transfer and friction testing [21,22]. The results of those studies indicated that the double dimple feature had marked improvements over the single dimple design. The overall channel Nusselt number and Nusselt number augmentation of the channels studied are shown in Fig. 2 and Fig. 3.

The Nusselt number augmentation is calculated as the ratio of the Nusselt number obtained with the dimpled channel divided by the Nusselt number predicted by the well-known Dittus-Boelter correlation for heating of the fluid. The friction factor augmentation is calculated as the ratio of the calculated Darcy friction factor by the friction factor predicted by the Blasius correlation. The double dimples (DD) are reported to have similar heat transfer augmentation comparable to the large dimples (LD) but with the lower friction factor augmentation (pressure lossspenalty) comparable to the small dimples (SD). The LD channel was also found to have the greatest Nusselt number augmentation at 30,000 Re, which was difficult to explain but was repeated in both studies. An explanation of the unique performance of the double dimple geometry as well as the peculiar LD geometry at 30,000 Re is the motivation for the flow visualization being performed in the current study.

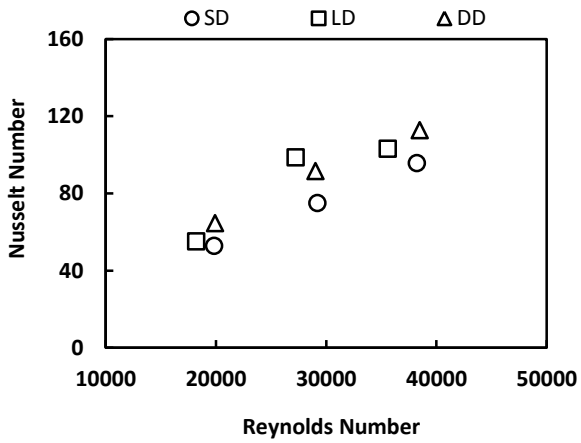

Figure 2: Averaged Nusselt Number of Dimpled Channel at Different Reynolds Numbers [22]

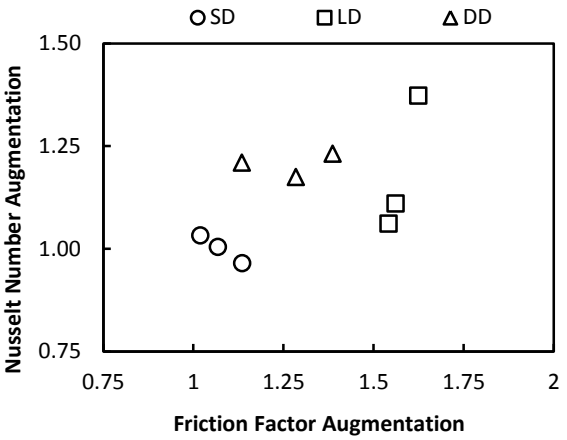

Figure 3: Overall Performance of Dimpled Channels [22]

Test Section

The test section and experimental setup used in this study is the same as that utilized in [16] but with some modifications. The current experimental setup is shown in Fig. 4.

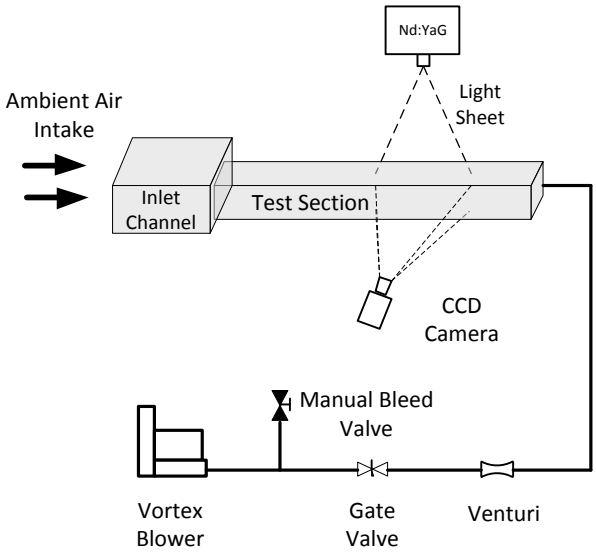

Figure 4: Complete Experimental Setup

The test section shown in Fig. 4 is a 4-walled acrylic channel, for clarity on the PIV setup, with an aspect ratio of 2. The channel width is 2" (5.08 cm), height is 1" (2.54 cm), and length is 30" (76.2 cm). Dimples are applied to one of the wide walls (other three walls left smooth) and arranged in a staggered setup seen in Fig. 5. The dimpled section starts immediately at the beginning of the acrylic test section. The test section contains a total of 27 rows of dimples. A 15 horsepower blower operates under suction where the flow is controlled with a gate valve and the flow rate is measured with a calibrated venturi flow meter. The inlet is open to atmospheric conditions. The particle seeding was added at the inlet channel through streamwise injection from a pressurized hose.

The parameters of the dimple geometries are listed in Table 1 below; a figure of their description is in Fig. 5. The large dimple has the largest dimple radius and dimple depth whereas the smalldimple has a smaller dimple radius and depth. The double dimple has an overall footprint betwen the large and small dimple. The double dimple geometry is two small dimples incorporated into one compound feature. The upstream and downstream dimple of the double dimple are identical and both have an equal radius to the small dimple that are offset in the streamwise position by 0.367d and aligned in the spanwise direction. The double dimple and small dimple arrays also have identical streamwise and spanwise pitch. The dimple density is also listed as a percentage of the projected flat area of the bottom wall covered by the overall dimple footprint.

Table 1: Geometric, Non-dimensional Dimple Parameters

Geometry	R/d	H/d	δ/d	P/d	S/d	Dimple Density
SD	**0.64**	**1.33**	**0.26**	**1.00**	**1.41**	**21%**
LD	**0.65**	**0.95**	**0.24**	**0.42**	**1.00**	**41%**
DD	**0.64**	**1.33**	**0.26**	**1.00**	**1.41**	**30%**

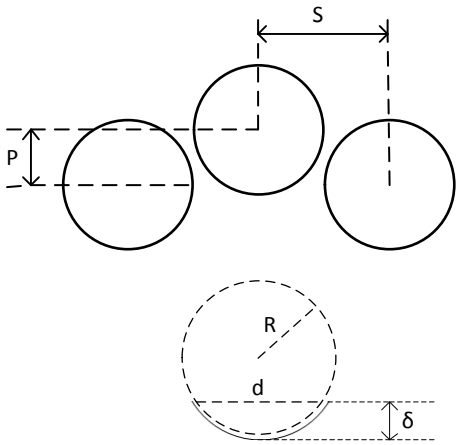

Figure 5: Description of Geometric Parameters

PIV Setup and Uncertainty

The primary PIV plane investigated in this paper is perpendicular to the dimpled features, denoted in Fig. 6. This plane was selected for investigation as it allows better visualization of the flow in and around the dimple. The relative positioning of the CCD camera and Nd:YAG laser can be viewed in Fig. 7. The viewing plane was positioned over the 17th dimple from the inletto ensure periodically fully developed flow. The featured wall was positioned perpendicular to the horizontal laser sheet. The camera was attached to a structure and suspended over the channel so that it could be focused on the perpendicular light sheet and view the xy plane over one full dimple period.

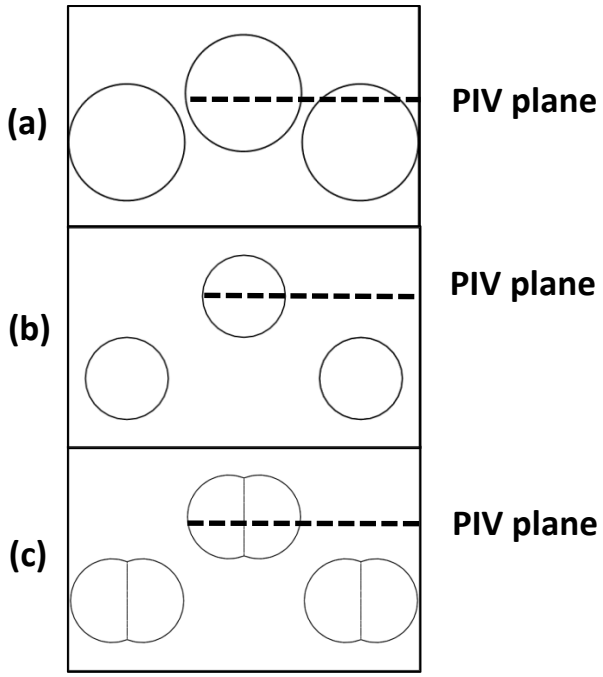

Figure 6: PIV Plane of Investigation for (a) LD (b) SD and (c) DD Geometries

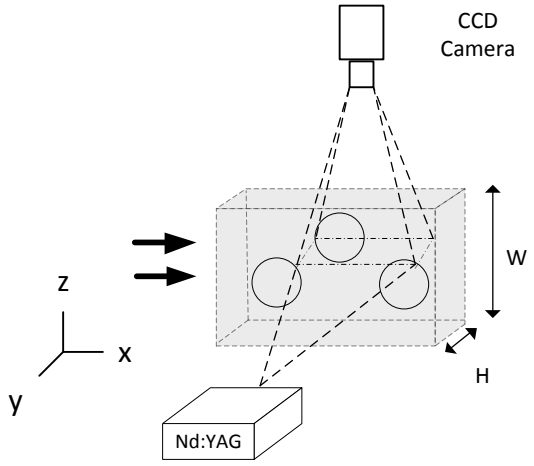

Figure 7: PIV Setup

The current experiment utilizes 2D PIV on a plane perpendicularly intersecting the center of the dimple footprint. Although 2D-PIV was restricted to a single mid-plane over the dimple feature in the fully developed portion of the channel as shown in Fig. 7, it is still possible to draw conclusions from the two-dimensional information to the strongly three-dimensional nature of the flow field.

A dual pulsed Nd:YAG laser with 70mJ/pulse energy was used for this experiment. A plano-convex lens was used to transform the 4mm circular beam into a diverging laser sheet. A CCD camera (LaVision Imager Intense, 1376 x 1040 resolution) was used for imaging. The CCD camera, operated at dual frame mode, was synchronized with the laser using a Portable Timing Unit. The maximum frame rate of the PIV system was 5 Hz. The flow was seeded with Bis(2-ethylhexyl) sebacate droplets (5μm average diameter). A set of 130 image-pairs were recorded for each case. The images were processed using DaVis software(by LaVision). Background subtraction was used to remove any scattered intensity from ambient. The vectors were generated using 32 x 32 pixel interrogation windows. The correlation function at a certain interrogation spot is given by Eq. (1):

$$R_{II}(x,y) = \sum_{i=-K}^{K} \sum_{j=-L}^{L} I(i,j).I'(i+x, j+y) \quad (1)$$

Where I and I' are intensity values in 1st and 2nd exposures respectively.

The highest peak of the aforementioned correlation function corresponds to the particle displacement. To screen out unreliable vectors, a threshold value for displacement to noise peak ratio was set to be 1.5, below which the displacement peak was discarded.

It can be shown that the random error associated with this kind of statistical mode of calculations decreases with the ratio of maximum displacement and linear size of interrogation window. However, an increase in displacement of particles also results in loss of correlation peak [29,30]. In the current experiment, the displacement was kept limited to 20 pixels, ensuring random error to be less than 2% in the case of the present 32x32 window size. Additional uncertainty arises from the size of the seeding particles. A smaller particle size will lead to increased bias error. On the other hand, the particle irregularities of larger seeding particles will lead to increased random error [31,32]. The experimental setup with the aforementioned camera resolution and seeding particle diameter used in our PIV measurements leads to a velocity uncertainty of ±0.5 m/sec (5% of the freestream velocity at the lowest Reynolds number).

Flow visualization using PIV measurements were performed for each dimple geometry at three channel Reynolds numbers (based on the projected smooth wall hydraulic diameter) of 20,000, 30,000, and 40,000.

It is important to mention that turbulence quantity measurements were not possible in the current experiment, because of the low framing rate of 5 Hz, the velocity fluctuation (U') could not be. Owing to this limitation in framing rate, the current work uses PIV as a tool only to understand the global flow structure. The authors also want to point out that measurements could not be made within the dimple feature cavity with the current experimental setup; the thickness of the light sheet and unwanted light scattering off the curved surfaces of the dimple resulted in intensity saturation in the field of view. In addition, poor optical access to the interior of the dimple also made it difficult to obtain accurate measurements within the cavity.

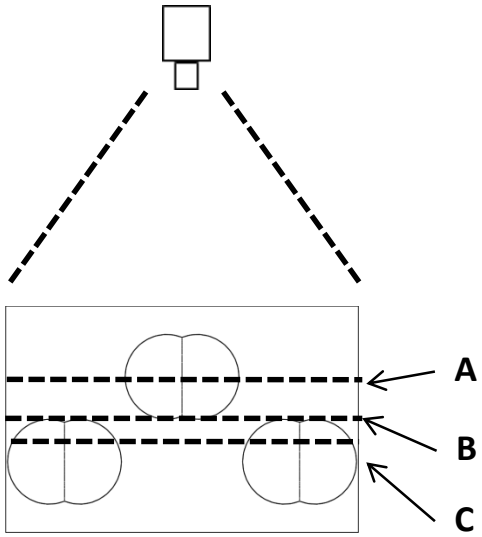

Figure 8: Dimple Planes

Key Features of PIV over a Dimpled Surface

PIV measurements were attempted on many planes as denoted in Fig. 8. A large amount of scattered reflection of the laser light occurred over the dimple concavity. The unwanted scattering cause a saturation of the measured intensity near the dimple. Even in the absence of seeding, the scattered light had such a strong intensity near the dimple that the background subtraction performed would have yielded meaningless data. Such scattering events were not observed in other test sections in the facility where PIV was previously applied and hence was not anticipated. In comparing planes A, B, and C in Fig. 8, planes B and C had overabundant light scattering, which saturated the CCD camera, hence the data was discarded. Only plane A provided meaningful results, which is the only plane presented in this paper. Note that Plane A denotes the same plane as shown in Fig. 6. The application of anti-reflecting coatings and use of additional optics to focus the laser sheet could allow for the other planes to be measured in future work.

Time-Averaged Velocity

The time-averaged, or mean, velocity field of the DD channel at all three Reynolds numbers tested is shown in Fig. 9. These averaged vector images only depict the time-averaged component of the velocity ($\bar{U}$). Figure 9 shows that the average freestream velocities are in the order of 10, 15, and 20 m/sec for Reynolds number 20,000, 30,000, and 40,000 respectively. These velocities are in agreement with the measured flow rate from the venturi (within the ±0.5 m/sec uncertainty of the particular experiment).

A dimpled wall results in more prevalent secondary flows, reducing the velocity magnitude near the dimples. To maintain the same mass flow rate, the maximum velocity region gets pushed towards the opposite wall. From Fig. 9, it is evident from the PIV data that the maximum velocity occurs not at the center, but in a location closer to the opposite wall. This shift

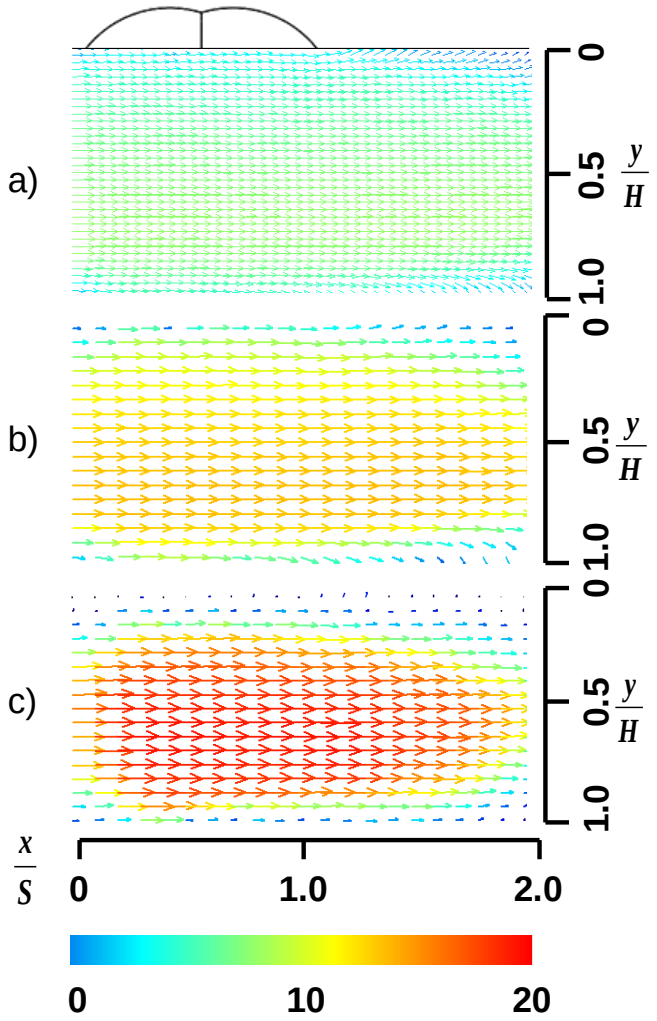

Figure 9: Mean Velocity Field (m/s) at Reynolds number a) 20000, b) 30,000 and c) 40000 of Double Dimple

causes sharper velocity gradients near the plane wall, resulting in some significant flow turning and vorticity generation on the opposite smooth wall.

Vorticity in the Flow Field

Vorticity has been selected as a parameter to reveal information about enhancement of mixing when the effect of turbulators on the flow field is being studied. Adding dimples to a channel has the potential to enhance mixing and thus the heat transfer. In order to understand the effect of different dimpled geometries on the mixing, the corresponding vorticity distribution was studied.

The vorticity field was calculated from the velocity vectors using a second order accurate finite differencing method. Although only one component of the vorticity could be resolved from 2D PIV, it reveals some interesting characteristics of the flow.

Additionally, the secondary flow structure near the dimpled wall is inherently unsteady. Instantaneous images of vorticity

and velocity vectors unveil that vortices generated by the dimple gets washed out towards the center of the channel and interacts with the main flow. Figure 10 also reveals that some of the vortices generated by the dimple are capable of propagating across and interacting with the opposite wall.

Instantaneous Flow Measurements

Although the measurements obtained accurately captures the velocity field at one instance, the sampling rate of the current study (5 Hz) is not suitable for charcterizing the vortex ejection, since they occur at smaller time scales. An examination of the instantaneous vorticity plots provides valuable qualitative insight to the location and intensity of turbulence production and dissipation within the channel. The vorticity contour of the DD channel at 30,000 Reynolds number at three consecutive instances is shown in Fig. 10. The vorticity near the featured wall is more prevalent than the opposite non-featured smooth wall at each instance. The flow disruption induced by the dimple can be seen in Fig. 9b with the change in the vortical structures. These instantaneous vorticity plots also show the presence of high vorticity zones near the dimpled wall. These localized high vorticity regions area result of the small vortices which are constantly generated and being ejected from the dimple. Figure 10 marks these phenomena of vortex ejection from the dimpled walls.

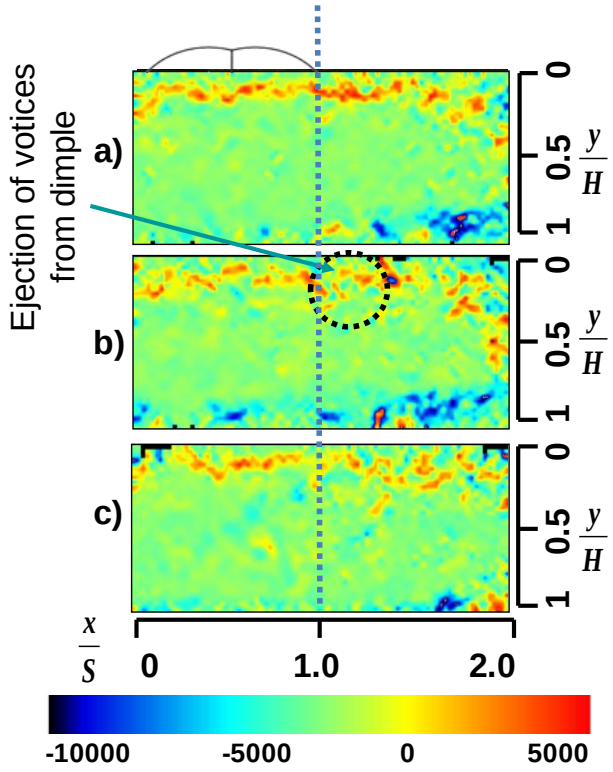

Figure 10: Instantaneous Vorticity (1/s) of Double Dimple at 30,000 Re and (a) 0 s (b) 0.2s (c) 0.4s

Although instantaneous vorticity figures provide some insight of the flow pattern, they do not reveal any quantitative information for comparison. The time-averaged vorticity plots can be more useful in this regard. The distribution of vorticity in the channel helps to better explain how the flow is being disturbed by the presence of the smooth and dimpled channel walls than looking at the velocity field alone and hence only plots of the time-averaged vorticity field are presented hereafter. The time-averaged vorticity of all three dimple geometries at all three channel Reynolds numbers are given in Fig. 11. A portion of Figs. 11a and 11b are shaded; these were regions of high saturation as previously discussed, where the accuracy of the data obtained was compromised.

Effect of Reynolds Number

As the Reynolds number increases, the vorticity near the walls also increases and the high vorticity zones are more widespread throughout the channel. The increase in fluid rotation near the walls can be explained by the fact that, with the increasing freestream velocity, the wall shear stress causing the fluid rotation also increases because of the greater velocity gradient. In comparing Figs. 11a-11c, the trend of increased vorticity with increasing Reynolds number was observed for all three geometries. The increased vorticity generated by the channel walls with increasing Reynolds number supports the increase in Nusselt number of the channels in Fig. 2 as reported in [21,22]. As the channel Reynolds number increases, the increased vorticity helps to promote greater mixing in the channel, resulting in the higher heat transfer at higher Reynolds numbers.

Comparison of Dimple Geometries

At 20,000 Re, the behavior of all three channels have very similar characteristics. Over the dimple cavity (approximately $0< x/S<1$), the high vorticity zones are confined to a small region near the wall. The shear layer that develops between the low momentum fluid in the cavity and freestream turns this region into a factory for turbulence. Hence, there is a correspondingly high vorticity in this region, where turbulence is being generated without large disruptions in the main flow.

Downstream of the dimple feature ($x/S > 1$), the vorticity is angled towards the channel centerline and is more diffused. The flow characteristics in this region are considerably different than the flow over the dimple cavity because of the ejection from the trailing edge of the dimple. The fluid ejected from the dimple trailing edge not only deflects the freestream flow towards the centerline, but also carries and transports the vortices generated from inside the dimple towards the centerline. Hence, in the region of $x/S> 1$, the mean vorticity breaks away from being parallel to the wall and is angled towards the centerline and becomes more diffused because of the interaction between the ejected fluid and freestream flow.

The vorticity near the featured wall of the DD and SD case is more concentrated than the LD (seen for all three Reynolds numbers). The vorticity of the LD case is more diffused and widespread, penetrating further towards the centerline of the channel. The differences in the mean vorticity of the three geometries help to explain the differences in their pressure drop

characteristics in Fig. 3; the LD had the greatest friction augmentation, whereas the SD and DD had similar friction. The widespread and diffused vorticity of the LD also helps to explain the large pressure drop (friction augmentation); the shearing action of the walls is able to penetrate further into the core of the flow because of the increased and widespread mixing being promoted by the LD. On the other hand, in the SD and DD, the vorticity is concentrated near the walls and hence the Reynolds shear stress and overall pressure drop in these channels is less. The similarities in the vorticity layers of the SD and DD also support how these channels exhibited similar friction.

It is worthwhile to note that over the conditions tested, the overall effect of the dimple is generally limited to half the channel height, consistent with results by Won et al. [25] where it was determined that the effects of dimples in altering time-averaged behavior occur mostly within one-half of one dimple print diameter from the surface.

Large Dimple Channel

In comparing Figs. 11a-11c, whereas the vorticity throughout the channel for the SD and DD behaved similarly at all three Reynolds numbers, the vorticity of the LD channel behaves differently and significant differences are observed between each Reynolds number. A careful consideration of the LD geometry helps to explain why this feature in particular behaved differently than the two smaller features.

The dimples in the LD case are the most closely spaced and have the closest proximity to one another (smallest P/d and S/d). They also have the greatest depth (smallest H/d) as well as the largest footprint, which also gives the dimples in the LD case the closest proximity to the nearest wall. Therefore, the LD is expected to have more vigorous flow interactions taking place in the channel than the two smaller features.

It is also important to note from Fig. 6 that, unlike the other geometries, in the LD case, a secondary dimple (the next dimple in the staggered array) intersects the measurement plane. A secondary dimple feature did not intersect the measurement plane for the DD and SD since they had a much smaller radius. The potential exists for the PIV to capture the influence of the next downstream dimple for all three geometries. However, that influence for the DD and SD will be much weaker than the LD because of the smaller size of those features and increased spanwise and streamwise pitch as well as the fact that there is a farther distance between the center of the secondary dimple and the measurement plane for the DD and SD cases. The measurement on the LD case is more likely to capture the additional effects of the secondary dimple and hence the flow field for the LD is expected to be even further different than the DD and SD.

At 30,000 Re, the entire flow field of the LD channel is active and the vorticity is widespread throughout the measurement plane, resulting in significantly enhanced mixing. The location at which the vorticity breaks away from being parallel with the wall is also moved upstream (to x/S = about 1). The early breakaway indicates a stronger ejection from the dimple. At 40,000 Re, the flow field in the LD channel changes. The breakaway location is no longer observed at 40,000 Re and the high vorticity region remains parallel to the wall. A further increase in vorticity did not occur at 40,000 Re for the LD. At this condition, the effect of the flow ejection from the dimple is diminished and the flow is likely being dominated by the other effects, the dimple-dimple flow interactions and the flow interactions between the dimple and the walls. Both of these effects are more prominent with the LD because of the larger footprint and smaller relative spacing of the LD feature as discussed earlier.

The extensive distribution of vorticity at 30,000 Re supports the highest heat transfer augmentation of the LD found at 30,000 Re. The lack of a further increase in vorticity and the change in the flow characteristics at 40,000 Re, which resulted in the loss of the enhanced mixing, also supports the lower heat transfer augmentation of the LD at 40,000 Re.

Small Dimple & Double Dimple Channel

A careful look at the vorticity of the SD channel in Figs. 11a-11c reveals that downstream of the dimple feature, the regions of high vorticity are deflected so strongly towards the centerline that a region of low vorticity is able to occupy the intermediate space between the high vorticity zone and the wall before the start of the next dimple (at high x/S and low y/H in the figure). On the other hand, the vorticity of the LD and DD channels do not exhibit this feature; the vorticity layers in the LD and DD channels do not detach from the wall.

The strong deflection of the vorticity in the SD can be explained by the shape of the dimple feature itself. The SD has a smaller radius than the LD, resulting in a steeper slope with respect to the channel walls at the leading and trailing edge of the dimple. The steeper slope (at the trailing edge) causes the vortices from within the small dimple to be ejected at a greater angle (towards the centerline) than the LD which has a greater radius. The deflection is slightly weaker, however, with the DD and further delayed because of the increased streamwise length of the DD feature.

The DD has an increased streamwise length because of the incorporation of two dimples into the feature and also contains a ridge between the upstream and downstream dimple that does not exist in the single dimple features. The presence of the ridge may disrupt the flow exiting the upstream dimple before being drawn into the downstream dimple. In addition, the increased streamwise length of the feature allows for the flow to enter and exit the dimple more gradually without being immediately ejected at a large angle.

The geometry of the feature is such that the generated vorticity is retained near the wall, promoting mixing near the wall. The near wall mixing brings colder fluid into close proximity of the hot wall and maintains a greater temperature gradient near the wall, the driving force of heat transfer to the cold fluid. However, heat transfer is more dependent on the local near wall mixing rather than the bulk flow, which the LD and DD accomplish better than the SD. These flow features of the double dimple help to explain how the DD is able to attain a

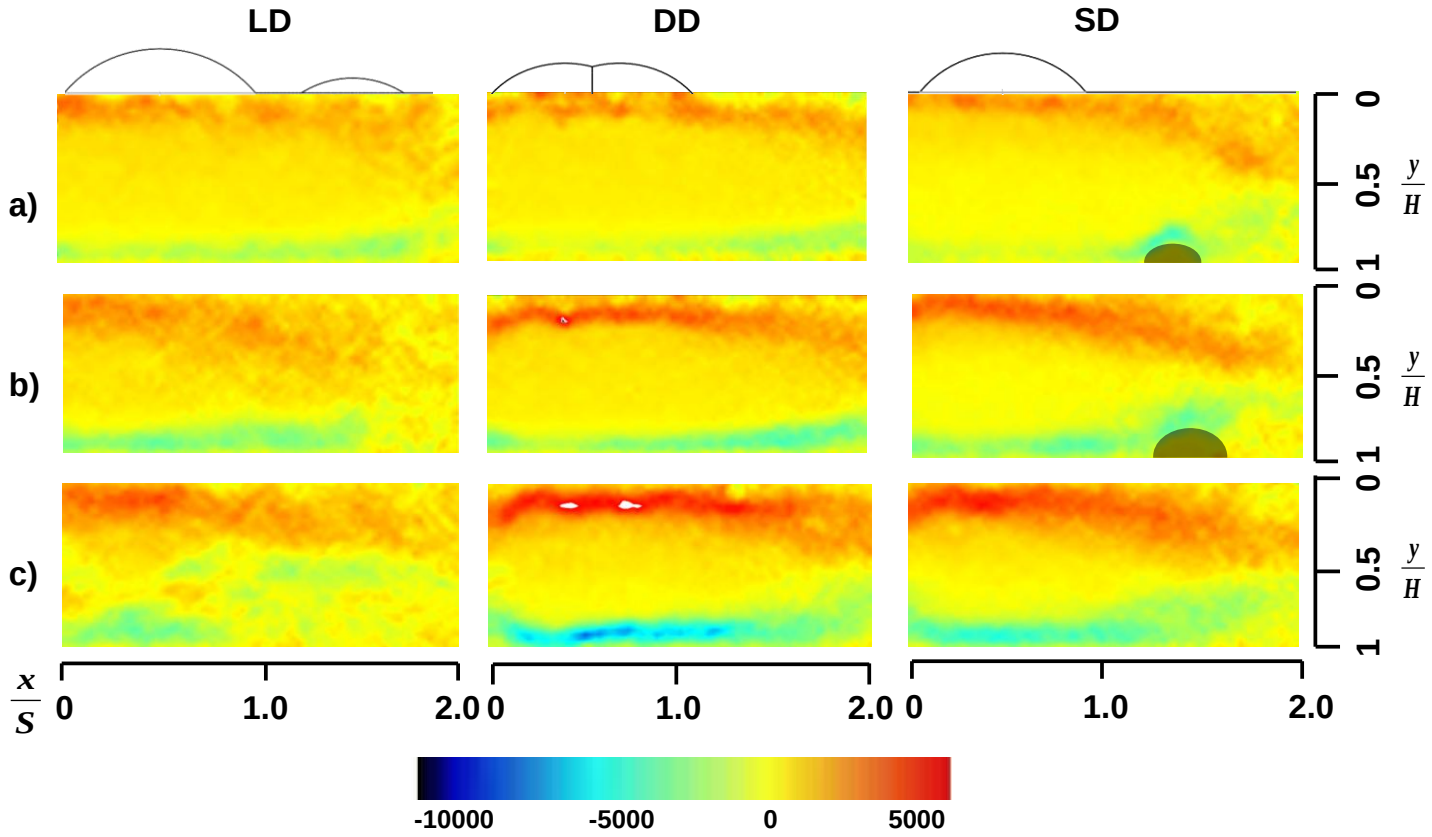

Figure 11: Mean Vorticity (1/s) of LD, DD, and SD at (a) 20,000 Re (b) 30,000 Re and (c) 40,000 Re

high heat transfer enhancement without a tremendous increase in friction augmentation, in reference to Fig. 3. Dimples can be considered a class of vortex generators, which are often employed to improve bulk mixing.

CONCLUSIONS

This paper attempts the first PIV results over a dimpled surface in an effort to understand the secondary flows and subsequent mixing cause by a dimple that leads to better thermal performance. In this investigation, the flow field in a 2:1 AR channel with dimples applied to one wall was studied using particle image velocimetry in order to provide explanations for trends observed in heat transfer and pressure drop results. PIV measurements were performed over the center of the dimple for three dimple geometries; a large dimple, small dimple, and double dimple. The flow field was investigated at three Reynolds numbers; 20,000, 30,000, and 40,000 for each dimple geometry.

The authors acknowledge that the current study is not completely representative of the flow field in the channel with only one measurement plane in the channel. After attempting to perform PIV measurements on other planes, it was determined that the thickness of the laser sheet made it difficult to obtain accurate measurements; unwanted light scattering off the curved surfaces of the dimple caused intensity saturation at key points in the field of view. Significant work can be done to improve the current experimental setup in order to obtain data on other planes. Such data would be valuable to others researching dimple-induced secondary flows. It can be added to the aforesaid that the flow field and heat transfer in a dimpled channel as well as within the dimple cavity, particularly the double dimple, needs to be investigated further.

The observed flow field is supportive of previously reported heat transfer results. The large dimple is observed to promote diffused and widespread vorticity (and hence mixing) throughout the channel. The vorticity in the double dimples and small dimples is localized near the wall, unlike the large dimples.

A change in the characteristics of the flow field was observed for the large dimple at higher Reynolds numbers but not the double dimple and small dimple geometries.

The unique performance of the double dimpled channel lies in its ability to retain the vorticity generated in the dimple closer to the walls, efficiently promoting turbulent mixing near the walls without additional increase in friction.

ACKNOWLEDGMENTS

The authors acknowledge the support from the Florida Center for Advanced AeroPropulsion (FCAAP). This work was performed at and with the support from students and staff of the Siemens Energy Center - a research laboratory at the University of Central Florida made possible through funds from Siemens Energy.

REFERENCES

1. Snedeker, R. S., and Donaldson, C. D., 1966, "Observation of Bistable Flow in a Hemispherical Cavity," AIAA Journal, **4**(4) ,pp. 735-736.

2. Murzin, V. N., Stoklitskii, S. A., and Chebotarev, A., 1986, "Creation of Solitary Vortices in a Flow Around Shallow Spherical Depression," Soviet Technical Physical Letters, **12**, pp. 547-548.

3. Belen'kiy, M. Y., Gotovskiy, M. A., Lekakh, B. M., Fokin, B. S., and Dolgushin, K. S.,1993, "Heat Transfer Augmentation Using Surfaces Formed by a System of Spherical Cavities," Heat Transfer Research, **25**, pp. 196-202.

4. Chyu, M. K., Yu, Y., Ding, H., Downs, J. P., and Soechting, F. O., 1997, "Concavity Enhanced Heat Transfer in an Internal Cooling Passage," ASME 42nd International Gas Turbine and Aeroengine Congress and Exposition, Orlando, FL.

5. Moon, S. W., and Lau, S. C., 2002, "Turbulent Heat Transfer Measurements on a Wall with Concave and Cylindrical Dimples in a Square Channel," GT-2002-30208, Proc. ASME Turbo Expo 2002, Amsterdam, The Netherlands.

6. Chyu, M. K., Yu, Y., Ding, H., 1999, "Heat Transfer Enhancement in Rectangular Channels with Concavities" Enhanced Heat Transfer, **6**(6), pp. 429-439.

7. Moon, H.K., O'Connell, T., Glezer, B., 2000, "Channel Height Effect on Heat Transfer and Friction in a Dimpled Passage," Journal of Engineering for Gas Turbines and Power, **122**(2), pp. 307-313.

8. Mahmood, G. I. and Ligrani, P.M., 2002, "Heat Transfer in a Dimpled Channel: Combined Influences of Aspect Ratio, Temperature Ratio, Reynolds Number, and Flow Structure," International Journal of Heat and Mass Transfer,"**45**(10), pp. 2011-2020.

9. Burgess, N. K., Oliveira, M. M., and Ligrani, P. M., 2003, "Nusselt Number Behavior on Deep Dimpled Surfaces Within a Channel," J. Heat Transfer. **125**(1), pp 11-18.

10. Burgess, N.K., and Ligrani, P.M., 2004, "Effects of Dimple Depth on Nusselt Numbers and Friction Factors for Internal Cooling in a Channel," GT 2004-54232, Proc. ASME Turbo Expo, Vienna, Austria.

11. Burgess, N. K.,and Ligrani, P. M., 2005, "Effects of Dimple Depth on Nusselt Numbers and Friction Factors," J. Heat Transfer. **127**(8), pp 839-847.

12. Isaev, S. A., Leontiev, A. I., Kudryatsev, N. A., and Pyshnyi, I. A., 2003, "The Effect of Rearrangement of the Vortex Structure on Heat Transfer under Conditions of Increasing Depth of a Spherical Dimple on the Wall of a Narrow Channel," High Temperature, **41**(2), pp. 229-232.

13. Griffith, T. S., Al Hadhrami, L., and Han, J.-C., 2003, "Heat Transfer in Rotating Rectangular Cooling Channels (AR=4) With Dimples," J. Turbomachinery, **125**(3), pp. 555-564.

14. Zhao, J. B., Chew, Y. T., and Khoo, B. C., 2004, "Experiemental Studies on Hydrodynamic Resistance and Flow Pattern of a Narrow Flow Channel with Dimples on the Wall," IMECE2004-59506, Proc. ASME International Mechanical Engineering Congress and Exhibition, Anaheim, CA, USA.

15. Borisov, I., Khalatov, A., Kobzar, S., and Glezer, B., 2004, "Comparison of Thermo-Hydraulic Characteristics for Two Types of Dimpled Surfaces,"GT2004-54204, Proc. ASME Turbo Expo 2004, Vienna, Austria.

16. Borisov, I., Khalatov, A., Kobzar S., Glezer, B., 2006, "Heat Transfer and Pressure Losses in a Narrow Dimpled Channel Structured with Spherical Protrusions," GT2006-90121, Proc. ASME Turbo Expo 2006, Barcelona, Spain.

17. Hwang, S. D., Kwon, H. G., and Cho, H. H., 2010, "Local Heat Transfer and Thermal Performance on Periodically Dimple-Protrusion Patterned Walls for Compact Heat Exchangers," Journal of Energy, **25**(12), pp. 5357-5367.

18. Leinhart, H., Breuer, M., and Koksoy, C., 2008, "Drag Reduction By Dimples? - A Complementary Experimental/ Numerical Investigation," International Journal of Heat and Fluid Flow, **29**(3), pp. 783-791.

19. Isaev, S. A., Kornev, N. V., Leontiev, A. I., and Hassel, E., 2010, "Influence of the Reynolds Number and the Spherical Dimple Depth on Turbulent Heat Transfer and Hydraulic Loss in a Narrow Channel," Int. J. of Heat and Mass Transfer, **53**, 178-197.

20. Leontiev, A.I., Isaev, S.A., Kornev, N.V., Chudnovsky, Y., and Hassel, E., 2010, "Numerical Modeling and Physical Simulation of Vortex Heat Transfer Enhancement Mechanisms over Dimpled Reliefs," IHTC14-22334, Proc. 14th International Heat Transfer Confernce, Washington, DC, USA.

21. Slabaugh, C.D, Tran, L. V., Ricklick, M., and Kapat, J.S., 2009 "A Study of Side Wall Heat Transfer Augmentation in a Narrow Rectangular Channel Duct," AIAA-2009-5377, Proc. 45th AIAA Joint Propulsion Conference, Denver, CO, USA.

22. Slabaugh, C.D, Tran, L. V., Ricklick, M., and Kapat, J.S., 2010, "Side Wall Heat Transfer Augmentation in a Narrow Rectangular Channel with Dimples Applied to the Bottom Wall," AIAA-2010-6953, Proc. 46th AIAA Joint Propulsion Conference, Nashville, TN USA.

23. Slabaugh, C.D., 2010, "Heat Transfer and Friction Augmentation in a Narrow Rectangular Duct with Dimples Applied to a Single Wall," University of Central Florida, Orlando, FL USA.

24. Mahmood, G. I., Hill, M. L., Nelson, D. L., Ligrani, P. M., Moon, H. K., and Glezer, B., 2001, "Local Heat Transfer and Flow Structure on and Above a Dimpled Surface in a Channel," J. of Turbomachinery, **123**(1), pp. 115-123.

25 Won, S. Y., Zhang, Q., and Ligrani, P. M., 2005, "Comparisons of Flow Structure Above Dimpled Surfaces with Different Dimple Depths in a Channel," Physics of Fluids, **17**, 045105.

26. Ligrani, P. M., Burgess, N. K., and Won, S. Y., 2005, "Nusselt Numbers and Flow Structure on and Above a Shallow Dimpled Surface Within a Channel Including Effects of Inlet Turbulence Intensity Level," J. Turbomachinery, **127**(2), pp. 321-330.

27. Terekhov, V. I., Kalinina, S.V. and Mshvidobadze, Y.M., 1995,"Flow Structure and Heat Transfer on a Surface with a Unit Hole Depression," Russ. J. Eng. Thermophys, **5**, pp. 11–34.

28. Terekhov, V. I., Kalanina, S. V., and Mshvidobadze, Y. M., 1997, "Heat Transfer Coefficient and Aerodynamic Resistance on a Surface with a Single Dimple," Enhanced Heat Transfer, **4**, pp. 131-145.

29. Scarano, F., and Riethmuller, M. L., 1999, "Iterative Multigrid Approach in PIV Image Processing with Discrete Window Offset," Experiments in Fluids, **26**, pp. 513-523.

30. Raffel, M., Willert, C., and Kompenhans, J., 1998, "Particle Image Velocimetry A Practical Guide," Springer-Verlag, Berlin Heidelberg.

31. Prasad, A., Adrian, R., Landreth, C., and Offutt, P., 1992, "Effect of Resolution on the Speed and Accuracy of Particle Image Velocimetry Interrogation," Experiments in Fluids, **13**, pp. 105-116.

32. Santiago, J. G., Wereley, S. T., Meinhart, C. D., Beebe, D. J., and Adrian, R. J., 1998, "A Particle Image Velocimetry System for Microfluidics," Experiments in Fluids, **25**(4), pp. 316-319.